ELSEVIER

Journal of Organometallic Chemistry 651 (2002) 80–89

Journal of Organometallic Chemistry

www.elsevier.com/locate/jorganchem

Characterization of a metallocene/co-catalyst system supported on silica by Fourier-Transform Raman spectroscopy

André van der Pol *, J.P.C. van Heel, Ramon H.A.M. Meijers, Robert J. Meier, Mirko Kranenburg

DSM Research, PO Box 18, 6160 MD Geleen, The Netherlands

Received 31 August 2001; accepted 21 January 2002

Abstract

2,2′-bis-(indene-2-yl)-biphenyl-Zirconium dichloride (biph[2-Ind]$_2$ZrCl$_2$) supported on silica and in the presence of methylaluminoxane (MAO) cocatalyst was studied by FT-Raman spectroscopy. Even though the transition metal was present at a concentration down to 0.12 wt.%, useful FT-Raman spectra were obtained. The aim of this work was to correlate spectral features to such typical catalyst properties like Al/Zr ratio and catalytic yield (CY). The Raman spectra contain signals due to the co-catalyst and the catalyst. Catalyst signals due to Zr–Cl, Zr–CH_3 and Zr-other ligand (e.g. Cp or Biph-2-Indene) bonds as well as ligand specific signals were identified using literature data, model compounds and ab-initio quantum chemical calculations of the vibrational spectra. An excellent correlation was found between the intensity ratio of the peaks at 3000 and 1500 cm^{-1} and the Al/Zr ratio. A fairly linear correlation was found between the signal intensity due to M–CH_3 bonds and the catalytic yield (kg PE per mmole Zr) for a series of samples of different Al/Zr ratios and different catalytic yields. © 2002 Published by Elsevier Science B.V.

Keywords: Zirconocene; Activation; Methylation; Catalytic yield; Vibrational spectroscopy

1. Introduction

In the last two decades catalysts for olefin polymerization derived from metallocene compounds and methylaluminoxane (MAO) as cocatalyst have attracted great interest both in academia and industry [1–4]. The metallocenes are single-site catalysts, as opposed to Phillips and Ziegler/Natta catalysts, which have been used already for many years commercially to produce polyolefins. Therefore, these catalysts produce a very uniform polymer with a narrow molecular weight distribution. Metallocene catalysts allow control of molecular weight, incorporation of co-monomer and tacticity. Furthermore, they are extremely active polymerization catalysts and have therefore raised the interest of polyolefin producers. The cocatalyst MAO can be described as a mixture of chains and rings comprised of the unit (–O–Al(CH_3)–). It is generally accepted that MAO activates the metallocene by alkylation and subsequent abstraction of one of the methyl or Cl groups, thus generating the catalytically active species: a metallocenium cation [5,6] (see Scheme 1). The mechanism of activation by MAO was studied recently in detail by ^{13}C-NMR [7] and UV–vis spectroscopy [8]. The uniqueness of MAO lies in its balance of its three properties: alkylation of the metal atom, abstraction of a methyl group, and stabilization of the created metallocenium cation.

In general, a homogeneous metallocene catalyst cannot be practically used for gas phase or slurry polymerization because of high reactor fouling. It is well known that it is possible to support these catalysts, e.g. on silica or alumina [9] offering the extra advantage of applicability in both gas phase and slurry reactors. The development of supported metallocene catalysts has been a very active area of research in the last decade. Much work devoted to preparation methods, interaction between catalyst and cocatalyst and the anchoring of metallocene catalysts to the surface of inorganic supports, has been published [10–13]. However, many aspects of supported metallocene interaction with alkyl-

* Corresponding author. Tel.: +31-46-476-7145; fax: +31-46-476-1200.

E-mail address: andre.pol-van-der@dsm.com (A. van der Pol).

0022-328X/02/$ - see front matter © 2002 Published by Elsevier Science B.V.
PII: S0022-328X(02)01258-5

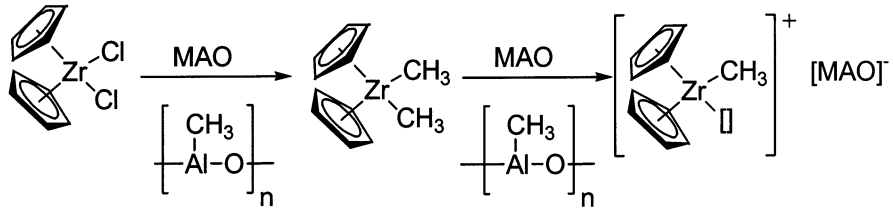

Scheme 1. Methylation of a zirconocene compound and cation formation.

aluminium co-catalyst, introduced into the polymerization medium, are still unclear.

In the current study we explore the use of FT-Raman spectroscopy to characterize the catalyst system 2,2′-bis-(indene-2-yl)-biphenyl-zirconium dichloride (biph[2-Ind]$_2$ZrCl$_2$, see Scheme 2 [14]). Despite the low amount of metallocene deposited on the MAO/Silica-support (0.1–0.4 wt.% Zr), we have anticipated that using Raman spectroscopy it might be possible to directly observe vibrations related to the 'active site' of the metallocene, i.e. the Zr–Cl and/or Zr–Me bond vibrations. This should make it possible to study the interaction of the metallocene with the MAO on the support, the disappearance of Zr–Cl bonds, the formation of Zr–Me bonds, and possibly the activation of the metallocene as a whole. Particularly, this might give us a tool to understand the difference between a 'good' and a 'poor' catalyst, on a molecular level.

A literature search (Chemical Abstracts) was carried out for the years 1969–1999, targeting papers with vibrational spectroscopic information on Cp$_2$ZrR$_2$ compounds and assignments of peaks. Relatively little has been published on this subject [15–23] compared with the very large number of papers dealing with synthesis of metallocenes and related polymerization experiments. The work described in references [15–19] concerns relatively simple compounds, with only cyclopentadienyl, chlorine and methyl ligands. The recent work of reference [20] contains some vibrational spectroscopic information on metallocene half sandwich complexes with pyridine containing bridges. However, the discussed Zr–Cl vibrations were interpreted based fully on the interpretation in ref. [18]. The other recent papers [21–23] all concern force field approaches, mostly involving fitting of parameters to simple species such as Cp$_2$ZrCl$_2$. No validation of these force fields for general metallocene type species was provided. Moreover, we need unbiased information on the activated, cationic, complexes, which in our view can only be reliably obtained by ab initio calculation. The spectroscopic region below 400 cm^{-1} contains only signals due to metal–ligand vibrations, while above 800 cm^{-1} signals due to the aromatic ligands can be found [19]. For the present work, the signals due to Zr–Cl and Zr–CH$_3$ stretching vibrations are the most relevant, they can be found in the regions 310–360 cm^{-1} [16–18] and 460–490 cm^{-1} [18] for Zr–Cl and Zr–CH$_3$ vibrations, respectively. Faced with the limited and sometimes dated information found in literature, we decided to support our assignment of vibrational peaks with ab initio calculations of vibrational spectra, both for the simple compounds as well as for the much larger biph[2-Ind]$_2$ZrCl$_2$ species. Both neutral dimethyl and monomethyl cation compounds were considered. At the time of the cited work of ref. [15–18], interpretation was primarily feasible using analogies to even simpler organometallic structures, and by making assumptions about, e.g., symmetry. For structures with other than very simple (halogens, methyl groups) substituents, however, the actual normal modes may well look very different. In the present work, the character of the normal modes may become more complex than simple bond stretching or angle bending. State-of-the-art first principles quantum mechanical calculations allow for a proper analysis of the vibrational modes in molecular systems, and such calculations have therefore been performed and the results are used in the present work to support the interpretation of the experimental results.

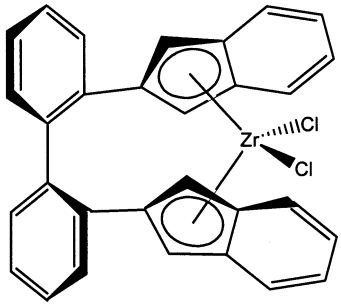

Scheme 2. Structure formula of 2,2′-bis-(indene-2-yl)-biphenyl-zirconium dichloride (biph[2-Ind]$_2$ZrCl$_2$) [14].

2. Experimental

For the biph[2-Ind]$_2$Zr-R$_2$ structure, due to the large number of atoms in the molecule, a complex Raman spectrum is expected, the spectrum of the supported catalyst/cocatalyst system will be even more complex. Therefore, pure MAO and MAO on silica were measured first before measuring the isolated biph[2-Ind]$_2$Zr-R$_2$ compound. The Raman peaks due to biph[2-Ind]$_2$Zr-R$_2$ were assigned to either the ligands or the metal-

chloride vibrations with help of spectra of the Li^+-ligand salt. Finally, the catalyst/cocatalyst sample supported onto silica was measured and the interpretation was accomplished using the results for the unsupported compounds, supported by theoretical calculations of the vibrational spectra.

2.1. Synthesis of the catalysts

All preparations were carried out under an atmosphere of purified nitrogen using standard Schlenk techniques. Solvents were carefully dried and freshly distilled from sodium–benzophenone prior to use. Silica (Grace Davison) was dehydrated with a nitrogen flow at a temperature of 200 °C. MAO was purchased as a 30 wt.% toluene solution (Albemarle). Solid MAO was prepared using a method described in a patent [24].

[2,2′-bis(2-indenyl)biphenyl]zirconiumdichloride was prepared according to a method described in ref. [25].

2.1.1. Supported [2,2′-bis(indene-2-yl)-biphenyl]-zirconiumdichloride

Silica (Grace Davison) was heated at 200 °C under a stream of nitrogen for 6 h. To 7 g of this silica 70 ml of toluene was added. The slurry was stirred and 50 ml of a 10 wt.% solution of methylaluminoxane (Albemarle) was added slowly. The resulting slurry was stirred for 16 h at room temperature (r.t.), after which the diluent was removed by evaporation at 30 °C. To a slurry of 2 g of the obtained solid (in 30 ml of toluene), a solution of 25 mg of the [2,2′-bis(indene-2-yl)-biphenyl]-zirconiumdichloride in 20 ml of toluene was added, and the resulting slurry was stirred overnight. The slurry was then decanted and dried by evaporation at 35 °C.

2.1.2. Polymerization

A 2 l stainless steel reactor was filled with 1 l heptane and 0.4 ml of a 1 M solution of tri-isobutylaluminium in toluene. The polymerization was carried out at 90 °C. Ethylene was added to the reactor with a total pressure of 15 bar. Slurry of the supported catalyst was prepared in a drybox, by weighing out 40 mg of catalyst and 10 ml heptane into a syringe. When the reactor reached the adjusted temperature and pressure, the catalyst slurry was injected into the reactor thus starting the polymerization. After 30 min of polymerization, the monomers were vented off, the polymer was collected and dried in a vacuum oven at a temperature of 50 °C. Table 1 lists information on the catalyst systems for which polymerization tests were carried out.

2.2. Raman measurements

Spectra were recorded, in backscattering geometry, using a Perkin–Elmer Spectrum 2000 NIR-FT Raman spectrometer (excitation wavelength 1064 nm, InGaAs detector). The samples were measured without taking them from their glass vials. The laser power was set at 200–400 mW (at the sample) and typically 200 scans were accumulated, leading to a total acquisition time of about 40 min. The spectral resolution was 4 cm^{-1}. Spectra were smoothed using a seven points moving average filter and the baseline was fitted through local minima and subtracted. All spectra were corrected for glass vial signals by subtracting a spectrum of an empty glass vial.

2.3. Theoretical calculations of the vibrational spectra

Two levels of theory, the Local Density Approximation (LDA) and the gradient corrected BP86 method, were applied to verify the method dependence of the results (which turned out to be small). Cp_2ZrCl_2 and Cp_2ZrMe_2 were calculated first to facilitate the interpretation of the spectral range 250–500 cm^{-1}.

The computations were performed using the PC SPARTAN Pro suite of programs [26], using a DN* basis set, and GAUSSIAN98 [27], using a LanL2DZ basis set, both running on an IBM Netfinity PC with pentium III processor (650 MHz). SPARTAN was used to compute the normal modes and frequencies for the larger systems reported in this paper. GAUSSIAN was used to calculate vibrational frequencies and intensities for the model systems Cp_2ZrCl_2 and Cp_2ZrMe_2 in order to validate the reliability of the methods employed when comparing to experimental spectra. The rationale regarding this is that with increasing size of the molecular system the number of molecular vibrations quickly rises, so for sufficiently large molecules there will 'always' be a calculated vibrational mode at a frequency near an experimental band. By calculating the Raman intensities, the required additional information is obtained which allows for a proper comparison between computation and experiment.

Density Functional Theory (DFT) based calculations were performed both at the LDA level as well as the BP86 Gradient Corrected level. Frequency computation was accomplished after full geometry optimization. The normal modes were inspected using either the SPARTAN graphical interface or GAUSSVIEW (GAUSSVIEW 2.1, Gaussian Inc, Pittsburgh, PA, 2000).

3. Results and discussion

3.1. Spectra of unsupported compounds

In Fig. 1, the Raman spectra of biph[2-Ind]$_2$Zr$(CH_3)_2$ and biph[2-Ind]$_2ZrCl_2$ are compared. The spectra are almost identical; only five clearly different peaks are observed, marked in the figure. These peaks are located at 454 and 1105 cm^{-1} for the dimethyl and at 308, 321

Table 1
Sample descriptions

Sample number	Al/Zr mol/mol	[Al] (wt.%)	[Zr] (wt.%)	Catalytic yield (kg PE per mmol Zr h)
1	107	12.8	0.40	51
2	151	12.8	0.29	133
3	204	12.8	0.20	142
4	299	12.8	0.14	264
5	350	12.8	0.12	282

All samples are $BiPh(2\text{-}Ind)_2ZrCl_2$ with MAO on SiO_2.

and 794 cm^{-1} for the dichloride compound. The peaks at 308 and 321 cm^{-1} are assigned to Zr–Cl symmetric and anti-symmetric stretch vibrations, while the peak at 454 cm^{-1} is likely due to Zr–CH_3 stretch vibration. The peak at 1105 cm^{-1} is assigned to the umbrella vibration of the methyl group. To aid in assigning the remaining peak positions the compound biph[2-IndLi^+]$_2$ was prepared and the Raman spectrum recorded (not shown). Clear peaks were revealed after careful baseline correction and by comparison to the peaks of biph[2-Ind]$_2ZrCl_2$ and biph[2-Ind]$_2Zr(CH_3)_2$ (see Fig. 1), 17 peaks can be assigned solely due to the biph[2-Ind]$_2$ ligand. These peaks are insensitive to the presence of Zr, Cl or CH_3. The next remaining peaks (39) are due to other than biph[2-Ind]$_2$ specific vibrations, for example an Ind-Zr vibration or due to biph[2-Ind]$_2$ ligand vibrations sensitive to the presence of Zr. The global assignments so far are compiled in Table 2.

We are particularly interested in peaks due to metal–chlorine and metal–methyl vibrations. Inspecting Table 2, it can be seen that the peak at 308 cm^{-1} is a good marker for Zr–Cl groups, while the peak at 321 is not. The latter peak is too close to the ligand specific peak, located at 322 cm^{-1}. The peak at 454 cm^{-1}, due to Zr–CH_3 groups, seems a good marker. The nearest peaks are located at 472 and 495 cm^{-1}. The peak at 1105 cm^{-1}, due to umbrella vibration of the methyl group, is too close to another (unassigned) peak at 1113 cm^{-1} to be a good marker (see Fig. 1).

In the next subsection the relatively simple assignments will be compared with theoretical calculations of vibrational spectra.

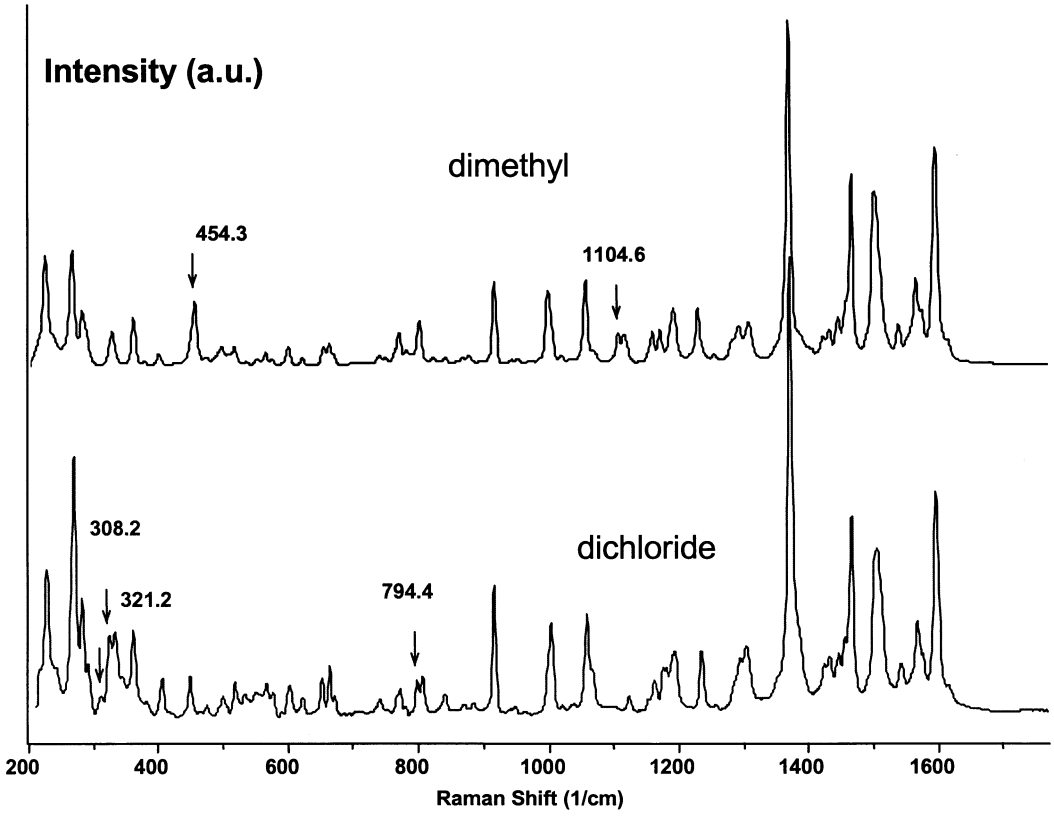

Fig. 1. Raman spectra of biph[2-Ind]$_2Zr(CH_3)_2$ and biph[2-Ind]$_2ZrCl_2$. Peaks unique to the compounds have been labeled.

Table 2
Global assignment of peaks in the Raman spectra of biph[2-Ind]$_2$ZrR$_2$ (R = Cl or CH$_3$) complexes

Peak positions (cm^{-1})	Assignment (chemical group)
308	Zr–Cl symmetric stretch
321	Zr–Cl anti-symmetric stretch
454	Zr–CH$_3$ stretch
794	Cl specific
1105	CH$_3$ specific, 'umbrella mode'
322, 330, 359, 600, 795, 913, 1001, 1056, 1065, 1190, 1232, 1291, 1302, 1463, 1502, 1565, 1594	BiPh[2-Ind]$_2$ specific (ligand)
221, 264, 280, 376, 398, 472, 495, 506, 515, 533, 550, 562, 573, 619, 652, 660, 668, 737, 747, 767, 779, 820, 838, 866, 875, 1016, 1113, 1157, 1168, 1252, 1276, 1329, 1367, 1420, 1429, 1442, 1536, 1572, 1612	BiPh[2-Ind]$_2$-Zr specific (entire metallocene compound)

3.2. Theoretical results

Our calculated results for Cp_2ZrCl_2 and Cp_2ZrMe_2 are collected in Table 3. Fig. 2 shows the experimental Raman spectra in the low wavenumber region obtained on solutions of these zirconocenes. On basis of calculations on Cp_2ZrCl_2 and Cp_2ZrMe_2, it turned out that the LDA (SVWN) frequencies agree better with experiment than the BP86 calculated values. For comparison we have given the BP86 calculated frequencies in brackets in the column 'Spartan' for species Cp_2ZrCl_2 in Table 3. The character of the mutually comparable normal modes was very much the same, and therefore we will now only report on the LDA calculated frequencies.

Inspection of the normal modes revealed that the Zr–Cl stretch vibrations are never pure stretch motions because these stretches exhibit counter-forces on the opposite Cp rings. Similar effects apply to the Zr–Me$_2$ stretch modes in Cp_2ZrMe_2. Thus the normal modes have a somewhat more complicated (e.g. not a pure Zr–C stretch) character when one compares to the interpretation provided in the older literature (cited above)

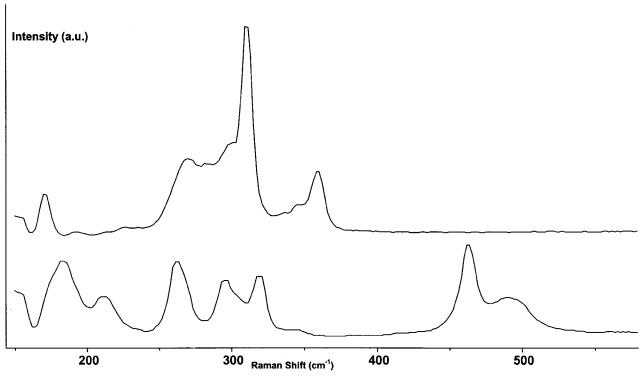

Fig. 2. Raman spectra of Cp_2ZrCl_2 (top) and $Cp_2Zr(CH_3)_2$ (bottom) in the low wavenumber region.

which, when one traces back the origin, is often based on group frequencies derived from very simple species such as MX_4.

The assignment on basis of LDA calculations is supported by Raman intensity calculations using Gaussian98W. For $ZrCp_2Cl_2$ we obtained the LDA frequencies, with the relative peak intensities given in brackets: 257(14), 278–281(18.5) and 308(21) cm^{-1}, which are to be compared with experimental peak positions and peak heights: 264 (7.5), range near 288 (7.1) and 310 (21) cm^{-1}. Noting differences in band widths, the agreement is satisfactory. In addition, between 350 and 1300 cm^{-1} only a single *strong* Raman band was calculated at 1143 cm^{-1}, which agrees well with the experimental value of 1127 cm^{-1}. This band is due to symmetric breathing of the Cp rings. In fact, two vibrational modes are closely spaced, which mutually breath in-phase or out-of-phase, respectively. Only one of the two exhibits the significant Raman intensity.

In the experimental system involving the biph[2-Ind]$_2$ zirconium complex supported on silica the zirconocene has been activated by reaction with MAO. The spectra may reveal vibrational bands arising from $ZrMe^+$ rather than from $ZrMe_2$. Therefore, initially, we have compared the calculated spectrum of Cp_2ZrMe^+ to that of Cp_2ZrMe_2. The results are also shown in Table 3. Almost all vibrations, which were obtained for Cp_2ZrMe_2 are also observed for Cp_2ZrMe^+. The differences in frequencies are of the order of the linewidths in the experimental spectrum, see Fig. 2. There is only one significant difference: the experimental band at 316 cm^{-1} for Cp_2ZrMe_2 experiences an upward shift by some 50 cm^{-1} for Cp_2ZrMe^+.

The calculations presented so far were felt a necessary step before moving to the biph[2-Ind] $_2ZrMe_2$, simply because computationally it would be too tedious to compute the *intensities* for that much larger system. Now that we have a proper comparison of the theoretical spectra of Cp_2ZrMe^+ and Cp_2ZrMe_2 involving both *frequencies and intensities*, we are ready for the next step, which involves computation of only the vibrational *frequencies* on the bis-indene-biphenyl zirconium complex. Using Spartan and LDA, we have thus computed the vibrational normal modes for 2,2′-bis-(indene-2-yl)-biphenyl-zirconium-dimethyl (biph[2-Ind]$_2$ZrMe$_2$), and for the cation biph[2-Ind]$_2$ZrMe$^+$. The theoretical assignments are given in Table 4. The most important result of this is the theoretical band at 469/461 cm^{-1}. This band (pure Zr–Me stretch) provides the scientific basis for our interpretation of the experimental band near 450 cm^{-1}, see Fig. 1. We relate this band to the presence of Zr–Me vibrations, irrespective whether this is the neutral or the cationic complex. Finally, we note that the energy minimized structure for the cation biph[2-Ind]$_2$ZrMe$^+$ revealed less symmetry than for biph[2-Ind]$_2$ZrMe$_2$, in particular one of the

Table 3
Experimental and calculated Raman frequencies and intensities for Cp_2ZrCl_2 and Cp_2ZrMe_2

$ZrCp_2Cl_2$			$ZrCp_2Me_2$			$ZrCp_2Me^+$	
Experimental (cm^{-1})	GAUSSIAN LDA (cm^{-1}, relative intensity)	SPARTAN (cm^{-1}) (BP86 frequency)	Experimental (cm^{-1})	GAUSSIAN LDA (cm^{-1}, relative intensity)	SPARTAN (cm^{-1})	GAUSSIAN LDA (cm^{-1}, relative intensity)	SPARTAN (cm^{-1})
264	257 (14)	257 (235) asymm. Zr–Cl+Cp tilting	259	250 (12)	257 Cp tilting	232 (6), 252 (17)	253, 258 Cp tilting
288	278 (5.5), 281 (13)	276 (252), 279 (258) both asymm. Zr–Cl+Cp tilting	288	286 (10)	273 Cp tilting	293 (6)	279 Cp tilting
310	308 (21)	310 (283) symm. Zr–Cl stretch+tilting Cp's	300	296 (4)	306 Cp tilting	308 (12)	323 Zr–Me+symm. Zr–Cp stretch
333 (rel. weak)	363 (1)	365 (343) asymm. Zr–Cl stretch+Cp tilting	316	307 (8)	321 Zr–Cp tilting+Me wagging	370 (3)	363 Zr–Cp stretch
353 (rel. weak)	371 (3)	373 (353) symm. Zr–Cl stretch+symm. Zr–Cp stretch	465	498 (20)	478 pure Zr–Me symm. Stretch	430 (3)	Band around 408 cm^{-1} (Me wagging) has different character compared with Gaussian calculated normal mode
			496	506 (3), 516 (8)	493 pure Zr–Me asymm. Stretch	486 (19)	486 Zr–Me stretch
1130	1143 ($\sim$100)	1154 (doublet) ring breathing	1129	1144 ($\sim$130)	1153 (doublet) ring breathing	1144/1152 ring breathing	1114 (doublet) ring breathing

For Cp_2ZrCl_2, the BP86 calculated frequencies are given, for comparison, between brackets in the column headed 'Spartan'. Raman intensities are given in $Å^4$.

indenyl frames becomes non-planar. The theoretical lack of frequencies in the range 500–530 cm^{-1} for the cationic complex, see Table 4, is attributed to this.

3.3. Spectra of supported compounds

Sofar, only spectra of pure catalysts have been presented. Obviously, it is very important that all components in a supported catalyst system can be identified separately in the spectra. Therefore, the spectra of pure MAO and of MAO on silica were recorded (not shown). The spectrum of MAO does not differ much from the spectrum of MAO on silica, apart from features due to the silica. In the spectra of MAO on silica a spectral window of low intensity can be observed, located around 480 cm^{-1}. This is very fortunate since in this window peaks due to $Zr–CH_3$ bonds are observed, see Table 2. Thus it offers a nice experimental handle for the observation of activation of catalysts where $Zr–CH_3$ bond formation might play a role.

Recently, Panchenko et al. have also studied the interaction of MAO with silica, using IR spectroscopy [28]. These authors focused on the region 2900–3700 cm^{-1}, in which –OH and C–H stretching signals can be observed. Since the spectrum of MAO did not change much upon supporting onto silica, it was concluded in that work that upon adsorption MAO does not change its structure. We have observed the same here, only now in a much broader spectral region.

Fig. 3 shows a comparison of the spectra (wavenumber region 200–1800 cm^{-1}) of biph[2-Ind]$_2$$ZrCl_2$, biph[2-Ind]$_2$$Zr(CH_3)_2$, biph[2-Ind]$_2$$ZrCl_2$ on MAO/Silica (sample 1, see Table 1) and of MAO/Si. The spectra have been scaled to the area of the C–H stretching signal due to MAO, located around 2900 cm^{-1} (not shown).

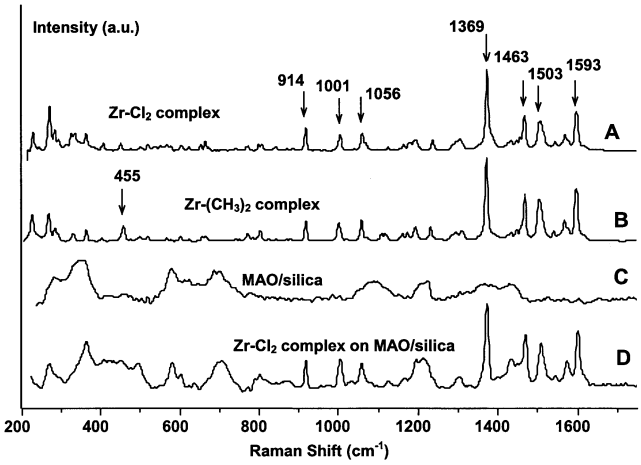

Fig. 3. Spectra of biph[2-Ind]$_2$$ZrCl_2$ (A), biph[2-Ind]$_2$$Zr(CH_3)_2$ (B), MAO/Silica (C), and of biph[2-Ind]$_2$$ZrCl_2$ on MAO/Silica (12.8 wt.% Al and 0.4 wt.% Zr). Many peaks due to the Indenyl ligands are insensitive to the support silica; the strongest peaks of these have been labeled in trace A. In the spectrum of the $Zr–(CH_3)_2$ complex (B) the peak due to $Zr–CH_3$ stretching vibration has been labeled (455 cm^{-1}).

The features due to the Zr complex are very pronounced in the spectrum of the supported system, although the concentration is only 0.4–0.12 wt.%. Signals due to the indenyl ligands can be recognized easily, some peaks have been labeled in the figure. Since the position and the relative intensity of these peaks seem unaffected by the MAO and the silica, these peaks can be used to determine the catalyst loading in unknown samples, see below. The spectral features due to MAO are rather broad, but can still be recognized in the spectrum of the supported catalyst system. As indicated in Fig. 3B (spectrum of the pure $Zr–(CH_3)_2$ complex), signals due to $Zr–CH_3$ stretching vibration are to be expected around 455 cm^{-1}. The spectrum of the supported catalyst indeed reveals a peak around this position. The spectrum of the supported sample was

Table 4
Theoretical (LDA) vibrational frequencies of the complexes biph[2-Ind]$_2$$ZrMe_2$ and biph[2-Ind]$_2$$ZrMe^+$ and experimental frequencies for biph[2-Ind]$_2$$ZrMe_2$ in the range 200–550 cm^{-1}

Normal mode description	Frequency for biph [2-Ind]$_2$$ZrMe_2$ (cm^{-1})	Experimental frequency, see Table 2 and Fig. 1	Frequency for biph [2-Ind]$_2$$ZrMe^+$ (cm^{-1})
Zr–Me stretch + Zr–Cp symm. stretch	256 (symm. Zr–Me stretch)	264	268
Zr–Cp antisymm. stretch + motion in entire ring system	282	280	294
Almost pure Zr–Cp stretch	296	Not observed	~308
Symmetric modes (likely Raman active) involving ring system	337 and 355	322 and 359	
Almost pure Zr–Me stretch	428 (antisymm. Zr–Me stretch)	423 (very weak)	440
Pure Zr–Me stretch	469 (symm. Zr–Me stretch)	454	461
Modes involving major Zr–Me stretch contribution	506, 510, 518, 529	495, 506, 515, 533	
Ring breathing like mode (doublet) in C_5 ring *and* biphenyl	~1030	997 and 1003	~1030

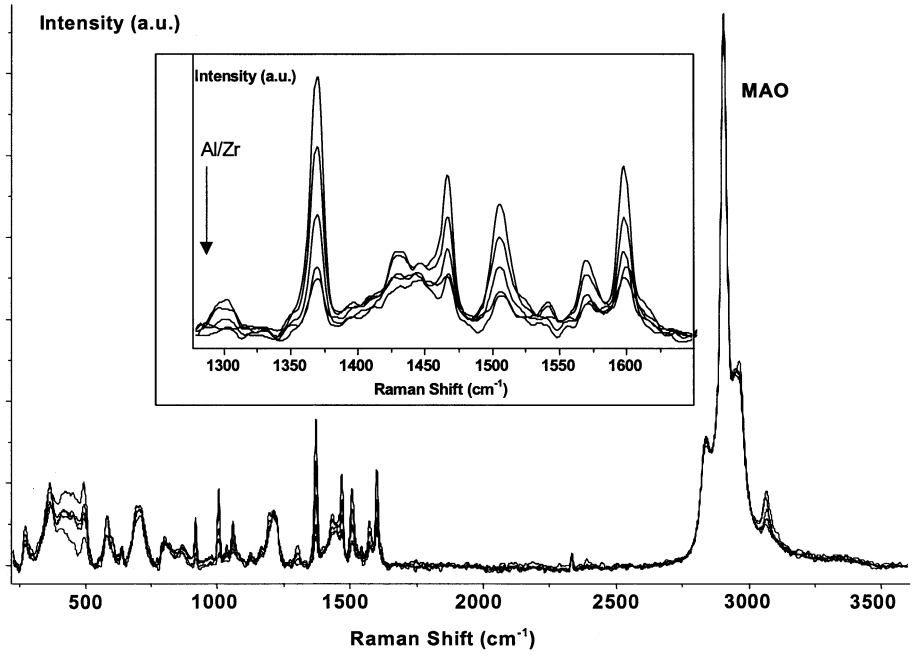

Fig. 4. Spectra of biph[2-Ind]$_2$ZrCl$_2$ on MAO/Silica (powders) for five different Al/Zr ratios (mol/mol): 107, 151, 204, 299, 350. The insert shows a close up of the region 1200–1700 cm^{-1}.

also inspected closely for peaks due to unconverted Zr–Cl bands, but none were detected.

In Fig. 4, the spectra of samples 1–5 are overlaid, see Table 1, (biph[2-Ind]$_2$ZrCl$_2$ on MAO/Silica). These samples differ in the ratio of Aluminium to Zirconium. The spectra have been scaled to the area of the strong MAO signal around 2900 cm^{-1}. This signal is representative for the total amount of Aluminium. The Al/Zr ratios were 107, 151, 204, 299 and 350, see Table 1. No very large differences are observed. The close-up also shown in the figure clearly shows differences, however. Peaks due to the Zr-complex can be observed, of which the intensity increases as the Al/Zr ratio decreases.

Fig. 5 shows a correlation plot of the ratio of integrated areas of the peaks due to MAO (integration boundaries 2746–3021 cm^{-1}) and Zr-complex (1489–1517 cm^{-1}). An excellent linear correlation is found (correlation coefficient $R^2 = 0.9991$), this means that for samples, after an initial spectral identification of the ligand, the Al/Zr ratio can be determined quantitatively from a relatively simple Raman measurement.

We now come to the most important finding to be reported here. Fig. 6 shows the region 300–600 cm^{-1} for spectra shown in full in Fig. 4, but now scaled to the area of the biph[2-Ind] ligand peak at 1502 cm^{-1}. A

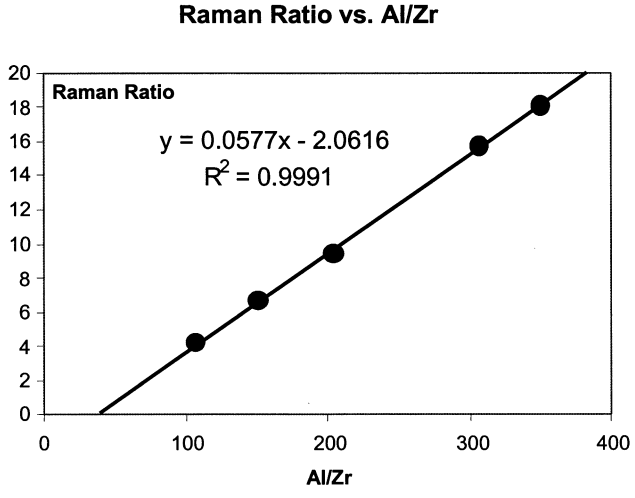

Fig. 5. Correlation between the Raman peak area ratio of the peaks at 3000 and 1500 cm^{-1} and the Al/Zr ratio and a fitted trendline.

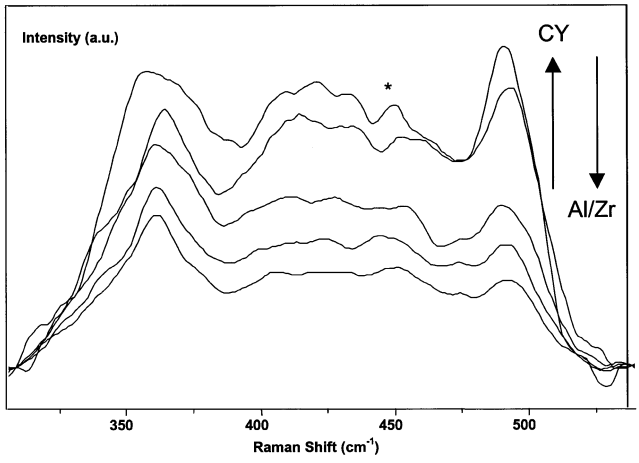

Fig. 6. Spectra of biph[2-Ind]$_2$ZrCl$_2$ on MAO/Silica (powders) for five different Al/Zr ratios (mol/mol): 107, 151, 204, 299, 350. The spectra are scaled to the intensity of the peak at about 1500 cm^{-1}. An asterisk marks a peak assigned to Zr–CH$_3$ vibrations.

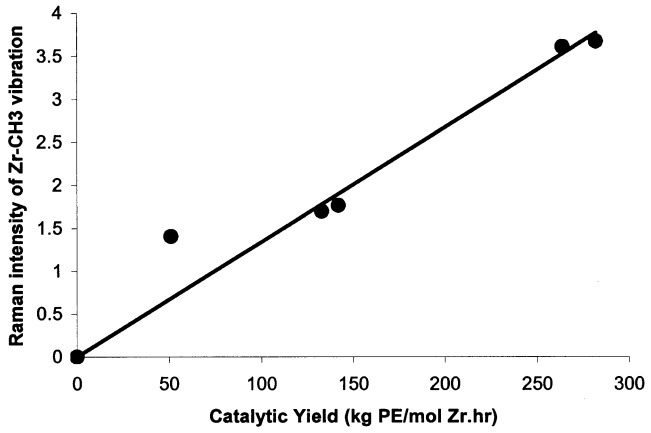

Fig. 7. Correlation between the normalized Raman peak height of the peak due to $Zr–CH_3$ vibrations, located at 454 cm^{-1}, and the catalytic yield in kg PE per mmol Zrh.

number of distinct peaks at slightly different frequencies can be observed in the 350–500 cm^{-1} region. The peak located around 454 cm^{-1}, which relates to vibrations primarily involving $Zr–CH_3$ stretch vibrations as corroborated from our ab initio calculations (Table 4), is marked by an asterisk. Furthermore, as the theoretical calculations of the spectra have shown, signals for $Zr–CH_3$ bands of the cationic complex can also be found in this region of the spectrum. The activity of a catalyst, as represented by the catalytic yield (CY) in kg PE per (mmol Zr h), must be proportional to the total amount of $Zr–CH_3$ bonds in the cationic complex biph[2-Ind]$_2$ZrMe$^+$. Consequently, in Fig. 7 we have plotted the intensity at 454 cm^{-1} versus experimental catalytic yield, CY (in kg PE per (mmol Zr h). A trendline, artificially drawn through the origin is also added, to help the readers eye. To obtain an estimate of the signal intensity due to $Zr–CH_3$ bonds, we derived the spectrum twice and determined from these second derivative spectra the absolute intensity, down to the baseline (at zero), in the region 415–470 cm^{-1}.

We observe a linear relation between the CY and the intensity. Apart from the datapoint at a CY of 50, which might be an outlier datapoint, the trend line more or less crosses the origin, meaning no catalytic yield for zero intensity (no active $Zr–CH_3$). It is also noteworthy that the other peaks located around 454 cm^{-1}, for example at 490 cm^{-1}, do also show a trend of increasing intensity for increasing CY, but the scattering is clearly higher. This latter observation also supports our assignment of the bands in the region near 450 cm^{-1}.

4. Conclusions

The Raman spectra of a metallocene/co-catalyst system supported on silica were studied.

Aided by ab initio calculations of the vibrational spectra of the actual system of interest biph-[2-Ind]$_2$ZrR_2, and by measurements on model compounds, peaks in the region 420–470 cm^{-1} are assigned to both the neutral dimethyl complex and the cationic monomethyl complex. From the Raman spectrum, the Al/Zr (i.e. the cocatalyst to catalyst ratio) can be predicted quantitatively. An excellent correlation is found between the intensity ratio of the peaks at 3000 and 1500 cm^{-1} and the Al/Zr ratio. A very satisfying correlation is found between the signal intensity due to Metal–CH_3 and the catalytic yield. This study shows that Raman spectroscopy is a potentially very powerful tool in the investigation of supported catalysts.

References

[1] A. Andresen, H.G. Cordes, J. Herwig, W. Kaminsky, Angew. Chem. 88 (1976) 689.
[2] G.G. Jordan, H.W. Turner, R.R. Eckmann, J. Am. Chem. Soc. 11 (1989) 2728.
[3] M. Bochmann, S.J. Lancaster, J. Organometallics 14 (1995) 3135.
[4] L. Resconi, L. Cavallo, A. Fait, F. Piemontesi, Chem. Rev. 100 (2000) 1253–1345.
[5] W. Kaminsky, M. Miri, H. Sinn, R. Woldt, Macromol. Chem. Rapid Commun. 4 (1983) 417–421.
[6] E. Gianetti, G.M. Nicoletti, R. Mazzocchi, J. Polym. Sci. 23 (1985) 2117–2133.
[7] I. Tritto, R. Donetti, M.C. Sacchi, P. Locatelli, G. Zannoni, Macromolecules 30 (1997) 1247–1252.
[8] D. Coevoet, H. Cramail, A. Deffieux, C. Mladenov, J.-N. Pedeutour, F. Peruch, Polym. Int. 48 (1999) 257–263.
[9] O.M. Kristen, Topics Catalysis 7 (1999) 89–95.
[10] T.J. Marks, Acc. Chem. Res. 25 (1992) 57.
[11] J.C.W. Chien, D. Hee, J. Polym. Sci. Part A: Polym. Chem. 29 (1991) 1603.
[12] W. Kaminsky, F. Renner, Macromol. Chem. Rapid Commun. 14 (1993) 239.
[13] G.G. Hlatky, Chem. Rev. 100 (2000) 1347–1376.
[14] EP99201856.4, DSM-Research, H.J. Arts, M. Kranenburg, R.H.A.M. Meijers, E. Ijpeij, G.J.M. Gruter, F.H. Beijer, Indenyl compounds for the polymerisation of olefins.
[15] P.M. Druce, B.M. Kingston, M.F. Lappert, T.R. Spalding, R.C. Srivastava, J. Chem. Soc. (A) (1969) 2106–2110.
[16] P.M. Druce, B.M. Kingston, M.F. Lappert, R.C. Srivastava, M.J. Frazer, W.E. Newton, J. Chem. Soc. (A) (1969) 2814–2816.
[17] E. Maslowski, K. Nakamoto, Appl. Spectr. 25 (1971) 187–191.
[18] E. Samuel, R. Ferner, M. Bigrogne, Inorg. Chem. 12 (1973) 881–887.
[19] E. Diana, R. Rossetti, P.L. Stanghellini, S.F.A. Kettle, Inorg. Chem. 36 (1997) 382–391.
[20] C. Schließburg, K.-H. Thiele, B. Lindner, W. Brüser, Z. Anorg. Allg. Chem. 626 (2000) 741–746.
[21] U. Höweler, R. Mohr, M. Knickmeier, G. Erker, Organometallics 13 (1994) 2380–2390.
[22] T.N. Doman, T.K. Hollis, B. Bosnich, J. Am. Chem. Soc. 117 (1995) 1352–1368.
[23] H.-H. Brintzinger, M.-H. Prosenc, F. Schaper, A. Weeber, U. Wieser, J. Molecular Structure 485-486 (1999) 409–419.
[24] EP 98204349.9, DSM-Research, R.H.A.M. Meijers, A. van Tol, M. Kranenburg, Process for the polymerisation of olefins.

[25] E.G. Ijpeij, F.H. Beijer, H.J. Arts, C. Newton, J.G. de Vries, G.-J.M. Gruter, J. Org. Chem. 67 (2002) 169–176.
[26] PC SPARTAN PLUS is available from Wavefunction Inc., 18401 Von Karman, Suite 370, Irvine, CA 92612, USA (pcsales@wavefun.com; http://www.wavwfun.com).
[27] GAUSSIAN98, M.J. Frisch, G.W. Trucks, H.B. Schlegel, G.E. Scuseria, M.A. Robb, J.R. Cheeseman, V.G. Zakrzewski, J.A. Montgomery, R.E. Stratmann, J.C. Burant, S. Dapprich, J.M. Millam, A.D. Daniels, K.N. Kudin, M.C. Strain, O. Farkas, J. Tomasi, V. Barone, M. Cossi, R. Cammi, B. Menucci, C. Pomelli, C. Adamo, S. Clifford, J. Ochterski, G.A. Petersson, P.Y. Ayala, Q. Cui, K. Morokuma, D.K. Malick, A.D. Rabuck, K. Raghavachari, J.B. Foresman, J. Cioslowski, J.V. Ortiz, B.B. Stefanov, G. Liu, A. Liashenko, P. Piskorz, I. Komaromi, R. Gomperts, R.L. Martin, D.J. Fox, T. Keith, M.A. Al-Laham, C.Y. Peng, A. Nanayakkara, C. Gonzalez, M. Challacombe, P.M.W. Gill, B.G. Johnson, W. Chen, M.W. Wong, J.L. Andres, M. Head-Gordon, E.S. Replogle, J.A. Pople, Gaussian, Inc., Pittsburgh PA, 1998.
[28] V.N. Panchenko, N.V. Semikolenova, I.G. Danilova, E.A. Paukshtis, V.A. Zakharov, J. Molecular Cat. A 142 (1999) 27–37.